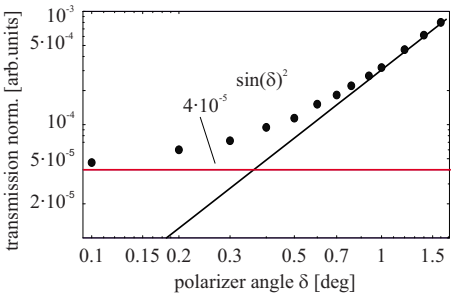

FIG. 4. (Color online) The extinction in cross-polarization with the ZnTe crystal of 1 mm thickness is determined from the crossing of maximum extinction and the sinus-square dependence of the transmission vs angle. The best achieved extinction levels in our experiments were 4×10^{-5}.

The use of 500 ps long Nd:YAG laser pulses facilitates the synchronization with the short CTR pulses and turns the EOA monitor into a very robust and quite easy to handle bunch length monitor. However, the required extinction levels of the cross-polarization arrangement to obtain a sufficient signal-to-background ratio for the long laser pulses have to be in the order of $10^{-5}-10^{-6}$. This is fairly difficult to achieve, since even the highest quality EO-crystals degrade the total extinction by about one order of magnitude due to strain induced birefringence. The best achieved extinction levels in our experiments were 4×10^{-5} (c.f. Fig. 4).

IV. BUNCH LENGTH MEASUREMENTS

After minimization of the extinction level with the ZnTe crystal in place has been obtained, the bunch length measurements are usually performed in two steps[9] as detailed out in the following.

A. Synchronization

Coarse synchronization to an accuracy of about 200 ps is achieved by overlaying the optical part of the TR, which passes through a central hole in the first out-coupling parabolic mirror, with part of the Nd:YAG laser pulses onto a PM (rise time ≤ 1 ns). The signal on the LIS detector can then be optimized by subsequent fine-tuning of the laser-CTR timing and the adjustment of both EOA interferometer arms to equal lengths. When optimum conditions for coincidence are accomplished, the recorded laser signal rises typically by a factor of 2–3 compared to the residual signal when no CTR is applied.

B. Signal analysis

If the longitudinal phase of the EOA interferometer is well adjusted, the spatial interference pattern can already be observed in the LIS raw data. However, the single-shot interference patterns $S(x)$ shown in Fig. 3 are the result of some basic data treatment according to Eq. (4), including background subtraction and normalization

$$S(x) = I_{\text{laser}}(x)\int [S_{\text{interf}}(\nu,x) - S_{\alpha\to 0}(\nu,x)]d\nu, \qquad (4)$$

where $S_{\text{interf}}(\nu,x)$ is the spatial fringe pattern of the broadband CTR expressed in Eq. (3) and $S_{\alpha\to 0}(\nu,x)$ is the horizontal profile on the LIS taken at an "out-of-phase" interferometer setting (large arm length difference) to emulate the profile resulting from the noninterfering CTR background. This is then subtracted to reveal the interference pattern.

Since this data treatment is done automatically by the experimental controls software package, shot-by-shot spatial autocorrelation profiles can be recorded in real-time during a measurement period, providing the possibility of tuning the LINAC's bunching section for shortest bunch lengths (Fig. 5).

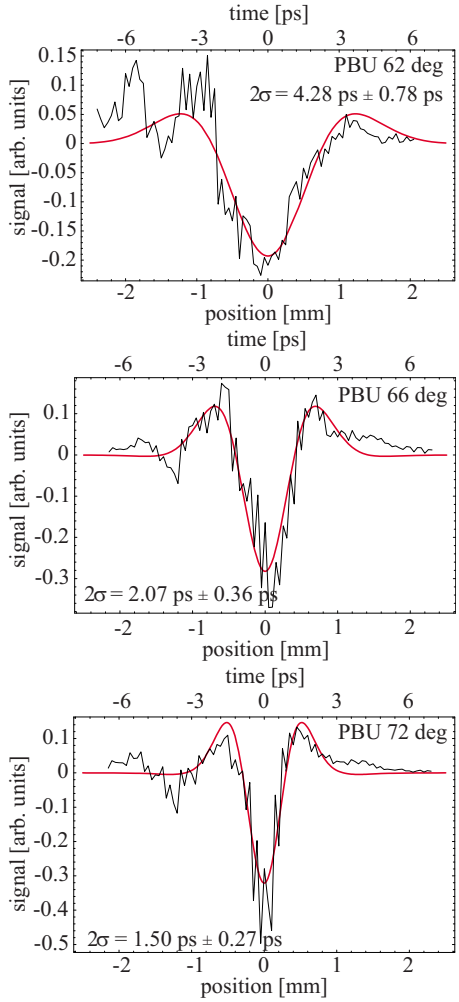

FIG. 5. (Color online) Single-shot, spatial autocorrelation profiles for different phase settings of PBU. Top: PBU phase of 62° results in a 2σ bunch length of 4.3 ps. Middle: PBU phase of 66° results in 2.1 ps. Bottom: PBU phase of 72° results in 1.5 ps. In all three cases, a simple Gaussian has been assumed for the longitudinal bunch configuration.

C. Bunch lengths versus prebuncher phase

In case of the short bunch operation mode of the SLS preinjector LINAC, both bunch length and energy spread depend quite sensitively on the relative phase settings of the three buncher cavities [500 MHz subharmonic prebuncher, four-cell (PBU), and 16-cell 3 GHz traveling wave bunchers]. The maximum CTR intensity was generated while maintaining a smooth energy distribution of the bunch. Although this LINAC optimization procedure may not always lead to the maximum CTR intensity, it justifies the assump-

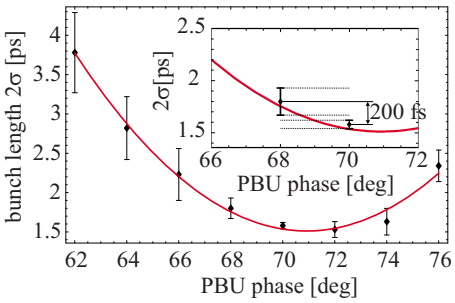

FIG. 6. (Color online) Average of ten single shots with standard deviation for different PBU phase settings. Minimum time resolution is in the order of 200 fs. The red line represents a quadratic fit.

tion of a Gaussian longitudinal profile for the EOA data analysis. Figure 5 shows autocorrelation profiles for different PBU settings, resulting in 2σ bunch widths between 1.5 and 4.3 ps assuming Gaussian longitudinal bunch configurations. The transfer functions of the experimental setup as well as the frequency dependent CTR and laser spot sizes have been considered in the data analysis [Eqs. (3) and (4)]. The fit parameters include the bunch length (2σ) and the intensity modulation depth of the recorded autocorrelation pattern $\alpha = \alpha_m \cdot \alpha_{eo}$. The quantity α_{eo} denotes the sensitivity of the electro-optical imaging system. α_{eo} describes the ability to translate the CTR intensity interference pattern into the polarization modulated transverse profile of the probe laser pulse and to sample this profile onto the detector. α_m is the interferometer modulation depth as given in Sec. IV B, depending on the intensities in the two signal arms. The fits have been achieved by using the build in function "NonlinearFit" in MATHEMATICA, which allows performing a least-squares fit to a list of data. The estimates of the model parameters are chosen to minimize the χ^2 merit function given by the sum of squared residuals $\Sigma_i e_i^2$.

Bunch length variations due to different PBU phase settings have been measured with a resolution down to 200 fs. The smallest deviation which is clearly distinguishable is in the order of 200 fs observed between a PBU phase of 68° and 70° as shown in Fig. 6 (cf., inset). This is in reasonable agreement with the theoretical optimum resolution of the present setup of 150 fs, which is determined by the 50 μm pitch of the pixel detector and the angle of incidence θ of the two signal arms of the interferometer [cf., Eq. (1)].

V. LIMITATIONS OF THE PRESENT SETUP AND FUTURE IMPROVEMENTS

The noninterfering CTR background is taken into account by subtracting a horizontal profile on the LIS taken at an out-of-phase interferometer setting (large arm length difference). In this context, we have identified the largest noise sources in the limited stability of the spatial profile of the probe laser system and the diffraction at the optics apertures as well as the pattern resulting from strain induced birefringence. The position stability of the probe laser system was measured to be in the order of ± 100 μm rms after the 15 m long optical transfer line.

The diffraction effects could be easily avoided using optics of larger diameter. The limited stability of the probe laser

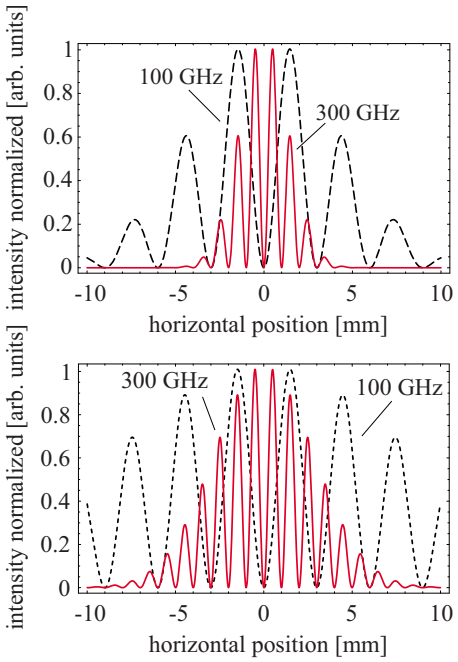

FIG. 7. (Color online) Finite size of the autocorrelation pattern due to the frequency dependent CTR spot size in the measurement plane of the interferometer for 100 and 300 GHz, respectively. The upper plot shows the pattern using a magnification factor of 1:1 while the lower plot is for a magnification factor of 2:1. The visibility of the outer interference fringes is clearly enhanced in the second plot.

is a distinct characteristic of a solid-state system which is hard to overcome. However, due to its unique design, a passively mode-locked Yb-doped fiber laser system offers greatly improved pointing stability and transverse beam quality. Furthermore, pulsed fiber lasers have been successfully locked to rf clocks with accuracies well below 100 fs.[10] Hence, using such a laser system with pulse durations of some ps should easily allow to retain the unique robustness of the monitor and to improve the signal-to-background ratio. We calculated that pulse energies in the order of 5 nJ are needed in an optimized setup. This should be obtainable with an Yb-doped fiber laser.

Another limitation of the present spatial interferometer lies in the fact that the size of the autocorrelation pattern is limited due to the frequency dependent finite CTR spot in the measurement plane. This leads to an inherent degrading of the modulation depth of the outer interference fringes. This cannot be overcome, however, by modification of the optical layout—magnification factor and convergence angle—the degrading of the modulation depth for increasing fringe orders can be adjusted. Note the clear advantage of this interferometer, the decay per fringe order stays constant for all frequencies. In the cases shown in Fig. 7, the fringe visibility is about 1/3 (second order fringes) for a magnification factor of 1:1 and 7/10 (second order fringes) for a magnification factor of 2:1. Here, it must be noted that a higher magnification factor leads to less intensity. The SLS LINAC is not predestined to produce shortest bunches with high beam charges (>1 nC). However, sufficient high radiation levels can be expected in future machines in order to produce autocorrelation patterns of good quality using higher magnification factors.

A. Sensitivity and signal-to-noise ratio

The sensitivity α of the EOA setup is defined by the intensity modulation depth of the interference fringes. α depends on the efficiency of both the interferometer and the electro-optical read-out. The latter describes the ability to translate the interference pattern into the polarization modulated transverse profile of the probe laser pulse and to sample this profile onto the detector (linear image sensor). The signal-to-noise ratio with respect to the final modulation depth α of the measured interferograms is defined by

$$S/N = (\alpha/\delta), \tag{5}$$

where δ is the noise background caused mainly by the limited stability of the probe laser beam and the strain induced birefringence in the ZnTe crystal as used in the experiment. The signal-to-noise ratio of the present setup is found to be in the order of 7 dB with respect to the characteristic zeroth order fringe.

The analysis shows that with a revised spatial interferometer setup (higher magnification factor of 2:1) and an improved electro-optical read-out (lower strain induced birefringence and better pointing stability of the laser system), the signal-to-noise ratio can be expected to improve by one order of magnitude. This in turn should enable to identify and measure higher order interference fringes.

VI. CONCLUSIONS

A novel, spatial EOA interferometer for single-shot bunch length measurements has been developed and successfully implemented at the 100 MeV SLS preinjector LINAC.[11] The long pulses of the Nd:YAG probe laser eases synchronization between electron bunch and laser resulting in a robust bunch length monitor. For different settings of the PBU prebuncher, electron bunch widths in the order of between 1.5 and 4 ps have been measured with subpicosecond time resolution.

The current setup has been successfully applied as an online monitor for the optimization process of the SLS preinjector LINAC for shortest bunches. Any change of the phase setting of the bunching cavities which leads to increased bunch lengths results in a widening of the interference pattern which thus can be easily traced. Therefore, the monitor described in this contribution represents an indispensable tool for an operator to optimize the machine for shortest bunches.

The monitor produces autocorrelation patterns of good quality. The zeroth order interference fringe is clearly visible in all of the recorded profiles. However, the signal-to-noise ratio is curtailed by the background of the EO read-out system and the Nd:YAG laser stability. Since the most stable pulses at the SLS LINAC are Gaussian shaped, without distinct longitudinal density modulations within the bunch, it is nevertheless sufficient to clearly reproduce the zeroth order interference fringe. The important quantity is the intensity modulation depth of the interference pattern. The present monitor setup has a signal-to-noise ratio in the order of 7 dB with respect to the zeroth order fringe. Thus, this is adequate to describe the bunches at the SLS LINAC in single-shot operation while demonstrating subpicosecond resolution by tracking bunch lengths changes as small as 200 fs.

However, for other machines, which produce non-Gaussian bunches with longitudinal density modulations on a subpicosecond basis, the visualization of the zeroth order fringe alone may not be sufficient. In this context, the side modulations of the interference pattern are becoming important. The largest improvements can be expected from a revised electro-optical imaging system. Particularly, a new setup could benefit from a more stable probe laser system as a major contribution in the noise background is due to fluctuations of the transverse profile of the laser. A fiber laser would offer much improved spatial stability due to its unique design. The stray light passing the cross-polarizer can be further reduced by using the shorter pulses of a fiber laser. An enhancement of the signal-to-noise ratio in the order of 10 dB is found to be possible. This would be sufficient to use the monitor at another machine which produces bunches with distinct modulations in their longitudinal shape.

ACKNOWLEDGMENTS

The authors wish to acknowledge the support by the Swiss National Science Foundation (SNF) Grant Nos. NFP-2100-061791.00/1 and NFP-200020-107858/1. Furthermore, the authors gratefully acknowledge the support from SLS staff during these experiments.

[1] M. Pedrozzi, M. Dehler, P. Marchand, L. Rivkin, V. Schlott, A. Streun, and C. Piel, Proceedings of the 2000 European Particle Accelerator Conference, Vienna, Austria, 2000, p. 851.
[2] D. Sütterlin, D. Erni, H. Jäckel, V. Schlott, M. Dehler, and H. Sigg, Nucl. Instrum. Methods Phys. Res. B **264**, 361 (2007).
[3] S. Casalbuoni, B. Schmidt, P. Schmueser, V. Arsov, and S. Wesch, Phys. Rev. ST Accel. Beams **12**, 030705 (2009).
[4] V. L. Ginzburg and I. Frank, J. Phys. (USSR) **9**, 305 (1945).
[5] D. Sütterlin, D. Erni, H. Jäckel, V. Schlott, H. Sigg, and A. Murk, Proceedings of the Seventh European Workshop on Beam Diagnostics and Instrumentation for Particle Accelerators, Lyon, France, 2005, p. 209.
[6] C. Hirschmugl, M. Sagurton, and G. Williams, Phys. Rev. A **44**, 1316 (1991).
[7] A. Murk, Research Report No. 2004-06 (University of Berne, 2004).
[8] See www.ticra.com for the General Reflector Antenna Software Package.
[9] D. Sütterlin, D. Erni, H. Jäckel, V. Schlott, H. Sigg, and A. Murk, Proceedings of the 2005 International Free Electron Laser Conference, Stanford, CA, 2005, p. 648.
[10] A. Winter, P. Schmueser, F. Ludwig, H. Schlarb, J. Chen, F. X. Kaertner, and F. Oemer Ilday, Proceedings of the 2006 European Particle Accelerator Conference, Edinburgh, Scotland, 2006, p. 2747.
[11] D. Sütterlin, Thesis No. 16668, ETH, 2006.